Kinetic Studies of Negative Ion Reactions in a Quadrupole Ion Trap: Absolute Rate Coefficients and Ion Energies

Edward R. Lovejoy* and Robert R. Wilson

NOAA Aeronomy Laboratory, 325 Broadway, Boulder, Colorado 80303

Received: October 21, 1997; In Final Form: January 28, 1998

A new apparatus consisting of an ion−molecule reactor coupled to a quadrupole ion trap is described. The kinetics and products of the rapid reactions of SF_6^- with SO_2, HNO_3, and HCl in the ion trap are reported. There is excellent agreement between the ion trap rate coefficients and yields, and flowing afterglow results. Rate coefficients for reactions of products of the SF_6^- reactions are also reported. Measurements of the equilibrium constant for the reaction $NO_3^-\cdot HNO_3 + HNO_3 \rightleftarrows NO_3^-\cdot(HNO_3)_2$ in the ion trap provide a very sensitive measure of the energy of the trapped ions. These measurements indicate that the effective temperature of the trapped $NO_3^-\cdot(HNO_3)_2$ ion is 320 ± 30 K for an ion trap at 298 K (1−2 mTorr He, $q_z = 0.074$). The presence of 0.2 mTorr N_2 buffer gas increases the internal temperature of the trapped ions by about 10 K. The internal temperature is also a weak function of the trapping potential, increasing by about 10 K over the range $0.074 < q_z < 0.286$.

Introduction

The Paul quadrupole ion trap[1] has become a very popular mass spectrometer due to its high sensitivity, versatility, and small size.[2] However, some of the subtleties of the ion trap performance are still not fully understood. One issue is the energy of the trapped ions. Trapped ions are translationally excited by the oscillating trapping potential. Quadrupole ion traps are usually operated with about 1 mTorr of He to damp the ions to the center of the trap, leading to enhanced sensitivity and resolution. Calculations suggest that in the presence of a light buffer gas the translational energy of trapped ions decreases to less than 1 eV after 15 collisions with He bath gas.[3] Vedel[4] calculates effective translational temperatures ranging from 500 to 5000 K for Cs^+ trapped in the presence of He buffer gas. Schaaf et al.[5] deduced a translational energy of several electronvolts from measurements of the Doppler profiles of Ba^+ trapped in 4×10^{-6} Torr He. The translational energy was about 10% of the trapping potential depth and decreased with increasing He pressure. Cutler et al.[6] reported a translational temperature of about 500 K for Hg^+ trapped in the presence of He, by measuring the second-order Doppler shift.

Lunney et al.[12] measured the temperature of K^+ ions in a Paul trap by analyzing the time-of-flight spectrum of the extracted ions. An energy of 0.3 ± 0.1 eV was obtained for 10^4 ions in a trap with a potential well depth of 60 eV and He buffer gas at 0.2 mTorr.

Energetic collisions with the buffer gas can lead to internal excitation of the trapped ions. The amount of internal excitation of trapped ions is not well established. Nourse and Kenttamaa[7] have deduced an effective O_2^+ temperature in a quadrupole ion trap with He buffer gas by comparing the rate coefficient and product yields for the reaction of $O_2^+ + CH_4$ with results from variable-temperature drift tube studies. Nourse and Kenttamaa conclude that the trapped O_2^+ ions have an effective temperature of 590−700 K. However, the distribution of the O_2^+ energy is uncertain because the reaction rate coefficient is sensitive to both translational and internal excitation.[8] Nourse and Kenttamaa also measured the rate coefficients for decomposition of protonated cyclohexene oxide and tetraethylsilane ions in the trap with He buffer gas. By assuming a form for the temperature dependence for the rate coefficient, Nourse and Kenttamaa deduced effective ion temperatures of 530−720 K.

Basic et al.[9] have studied the kinetics of the reactions $Ar^+ + N_2$ and $O_2^+ + CH_4$ in a quadrupole ion trap. The rate coefficients for both reactions have significant energy dependencies, and comparison of the measured rate constants with flow drift data yields effective ion energies. Basic et al. report Ar^+ and O_2^+ center-of-mass kinetic energies in the range 0.1−0.3 eV in the ion trap for a variety of experimental conditions. Brodbelt-Lustig and Cooks[10] have found very good agreement between relative basicities measured by the proton-transfer equilibrium technique in an ion trap with thermal measurements, suggesting that the effective ion temperature is close to the trap temperature.

McLuckey et al.[11] measured the decomposition rate coefficients for protonated water and methanol clusters in an ion trap mass spectrometer with 0.02−1.2 mTorr He buffer gas. They estimated that the ion internal temperatures were less than 1000 K on the basis of known thermochemical parameters and the measured decomposition kinetics. They also found that the ion temperature increased as the trap pressure decreased.

In the present work, a new apparatus consisting of an ion−molecule reactor coupled to an ion trap mass spectrometer is described. Rate coefficients for the rapid reactions of SF_6^- with SO_2, HNO_3, and HCl are measured in the trap and compared with the thermal rate coefficients. The kinetics of some of the product ions of these reactions are also measured. These studies demonstrate that the ion−molecule reactor/ion trap combination is a very versatile apparatus for studying ion−molecule kinetics. In addition, the kinetics of the formation and the decomposition of $NO_3^-(HNO_3)_2$ are studied in the trap as a function of pressure, bath gas, and trapping potential. These studies yield the effective temperature for the trapped $NO_3^-(HNO_3)_2$ ion.

S1089-5639(97)03391-4
Published on Web 03/07/1998

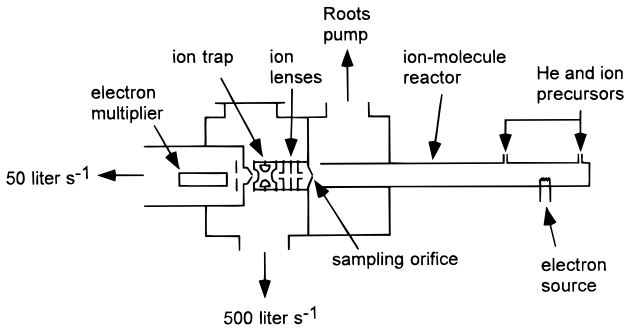

Figure 1. Ion−molecule reactor/quadrupole ion trap mass spectrometer apparatus.

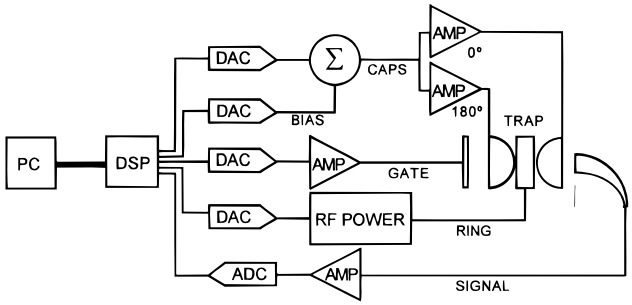

Figure 2. Ion trap control electronics.

Experimental Section

Experiments were performed with an ion−molecule reactor coupled to a quadrupole ion trap mass spectrometer. The apparatus is shown in Figure 1. The ion−molecule reactor consists of sections of 3.4 cm i.d. stainless steel tubing connected with metal-sealed knife-edge flanges to make an overall length of about 100 cm. The reactor is equipped with several gas addition ports and an electron source. The reactor temperature is regulated by flowing thermostated fluid through copper tubing soldered to copper foil wrapped around the reactor. Electrons are produced with a heated thoriated iridium filament at the upstream end of the reactor, and negative ions are produced by electron attachment to gases added to the main He flow. Reactor pressures range from 1 to 20 Torr with a main He flow rate of about 100 STP cm^3 s^{-1} (STP = 1 atm, 273 K), giving reactor residence times of about 10−200 ms. The ion−molecule reactor is pumped with a Roots blower backed by a mechanical pump.

A small fraction of the ion−molecule reactor gas is sampled through a Ni aperture (0.25 mm diameter) into the ion trap chamber. The ion beam is focused into the ion trap by a set of three lenses mounted behind the sampling aperture. The aperture, lenses, and ion trap are individually biased with a multichannel dc power supply (±150 V). Ions are gated into the trap by controlling the bias of the first lens. The ion trap has an internal radius of 1 cm and stretched end cap geometry. Each end cap has a 1.2 mm diameter centered aperture. Ions ejected through the exit end cap pass through an aperture (4 mm diameter) into a differentially pumped chamber and are detected with a discrete dynode electron multiplier equipped with a conversion dynode. The electron multiplier chamber and the ion trap chamber are pumped by 50 and 500 L s^{-1} turbomolecular drag pumps, respectively. The trap chamber pressure is measured with a capacitance manometer and is corrected for thermal transpiration.[13] Typical ion trap pressures are 0.2−2 mTorr He. The pressure in the detector chamber is about 20 times lower than in the ion trap chamber. Ion trap parameters of $r_0 = 1$ cm and $f = 1.01$ MHz give a relationship for the trapping parameter of $q_z = 0.0479V_{p-p}/m$, where V_{p-p} is the peak-to-peak rf voltage and m is the ion mass in amu.[2] Flow rates are measured with mass flow meters calibrated by measuring the rate of pressure change in a calibrated volume. Pressures are measured with capacitance manometers.

The ion trap is controlled by in-house-built electronics. The ion trap control electronics are diagrammed in Figure 2. This system controls the ring electrode rf voltage, the lens gate bias, and end cap waveforms and acquires data during the mass scan. Two different types of waveforms are applied to the ion trap end caps. Filtered noise fields (FNFs),[14] are used for mass filtering during the ion-trapping period, and sine waves are used for axial modulation during the mass scan. These waveforms are generated by a multichannel synchronous waveform generator, which also controls the amplitude of the ring electrode rf voltage, the end cap bias voltage, and the ion lens gate. The rf amplitude, end cap bias, and gate are controlled by 12-bit digital to analog converters (DACs). The end cap waveform is provided by a high-speed 8-bit DAC, which is routed through a smoothing filter, rf transformer, and finally into two power amplifiers. The maximum amplitudes of the rf, end cap excitation, cap bias, and gate are ±2500, ±12, ±12, and ±90 V, respectively.

The data acquisition electronics consist of a discrete dynode electron multiplier, a preamplifier (10^{-6} A/V), a 16-bit analog to digital converter (ADC), and 16 kB of memory. The ADC samples the signal every 10 μs during the mass instability rf scan, in synchronization with the steps in the ring electrode rf amplitude. The digitized signal is stored chronologically in static memory until it is either read back or overwritten by the next data gathering cycle.

The ion trap electronics are controlled by a dedicated digital signal processor (DSP). A standard PC is interfaced to this processor via a high-speed parallel port cable. Custom macro-driven software allows the user to adjust the timing and amplitude of the rf voltage, the gate, and the end cap waveforms. The ion trap runs continuously once these parameters are downloaded to the DSP. Data are stored at the end of each cycle and returned to the microcomputer over the high-speed parallel port cable. The mass spectra are displayed graphically on the PC.

Results

Ion Trap Chamber Conductance. The mean free path of He at 1 mTorr and 300 K is about 15 cm, which is a significant fraction of the dimensions of the ion trap chamber. For these conditions the flow through the chamber is intermediate between slip and molecular,[15] and the conductance is a function of the mass of the gas. The conductance is less for heavier gases, leading to an enhancement of the partial pressure of the heavier gases above that calculated from the partial flow rate of gas into the trap chamber. The enhancement was quantified by measuring the change in pressure in the ion trap chamber as a function of flow rate of added gas for a variety of gases. A constant flow of He was maintained into the chamber to give a pressure between 1 and 2 mTorr, and the pressure change above the He background was measured per unit flow rate of the heavier gas. The chamber pressure increased linearly with flow rate of added gas for pressure increases up to 0.5 mTorr. The measurements are summarized in Figure 3. The enhancement factor is defined as the change in chamber pressure per unit flow rate into the chamber relative to the change in pressure by He for the same unit flow rate. It should be emphasized that the enhancement factors are probably instrument specific, so

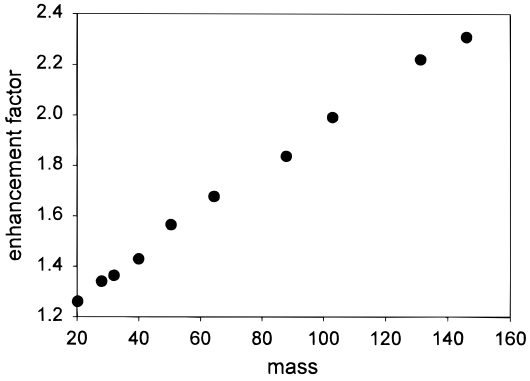

Figure 3. Ion trap concentration enhancement factors as a function of mass. The gases are Ne, N_2, O_2, Ar, CH_3Cl, C_2H_5Cl, CF_4, $CHFCl_2$, Xe, and SF_6, in order of increasing mass.

that the factors measured in the present work are not applicable to other systems.

The gas conductance differences lead to an enhancement in the concentration of heavier gases in the ion trap. In an excess of He the concentration of gas X (molecule cm^{-3}) in the ion trap chamber is given by

$$[\mathrm{X}] = \frac{EF_x^{\mathrm{STP}}P9.66 \times 10^{18}}{F_t^{\mathrm{STP}}T} \qquad (1)$$

where E is the enhancement factor (Figure 3), P is the ion trap chamber pressure (Torr), T is the temperature (K), F_x^{STP} is the flow rate of gas X into the chamber at standard conditions, and F_t^{STP} is the total flow rate of gas into the chamber, including the flow from the ion−molecule reactor. The flow of He from the ion−molecule reactor into the ion trap chamber was determined by measuring the ion trap chamber pressure with no other He added and comparing with measurements of the chamber pressure versus known added He flow. The flow rate of He from the ion−molecule reactor was typically about 10% of the total flow rate into the ion trap chamber.

SF_6^- and Product Ion Kinetic Measurements in the Ion Trap. Rate coefficients for the rapid bimolecular reactions of SF_6^- with SO_2, HNO_3, and HCl were measured in the trap. SF_6^- was generated in the ion−molecule reactor by electron attachment to SF_6. SF_6^- ions were loaded into the trap by gating the first electrostatic lens for several milliseconds, and then isolated by using a selective noise field applied to the end caps. Reactant gases were added to the trap chamber with He. The SF_6^- and product ion signals were measured as a function of time following the selective trapping of the SF_6^-. Typically, 10 trap−react−scan cycles were averaged for each delay time. An example of the temporal variation of the SF_6^-, FSO_2^-, $F_2SO_2^-$, and SF_5^- signals in the presence of SO_2 is shown in Figure 4. The slope of the SF_6^- decay gives the pseudo-first-order rate coefficient for loss by reaction with SO_2. Pseudo-first-order rate coefficients for SF_6^- loss are plotted as a function of the concentration of SO_2 in Figure 5. The slope of this plot gives the second-order rate coefficient for the reaction $SF_6^- + SO_2$. The rate coefficients for reactions of SF_6^- with HNO_3 and HCl were measured using similar methodology as for $SF_6^- + SO_2$. These results are also summarized in Table 1.

HNO_3 was metered into the ion trap chamber by flowing He over concentrated HNO_3 held in a Pyrex reservoir at 273 K or at room temperature. The HNO_3 concentration was controlled by varying the He flow rate through the reservoir and the flow of He added downstream. The HNO_3/He mixture flowed

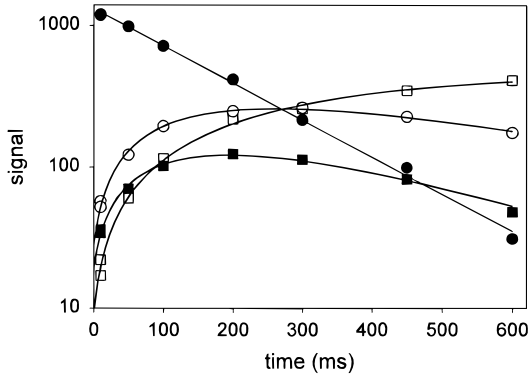

Figure 4. Variation of SF_6^- (filled circles), $F_2SO_2^-$ (open circles), SF_5^- (filled squares), and FSO_2^- (open squares) with reaction time for $[SO_2] = 6.7 \times 10^9$ molecule cm^{-3}, 1.5 mTorr He, and $290V_{p-p}$ trapping voltage. The lines are fits to the data based on a mechanism involving the reactions of SF_6^-, $F_2SO_2^-$, and SF_5^- with SO_2 (Table 1).

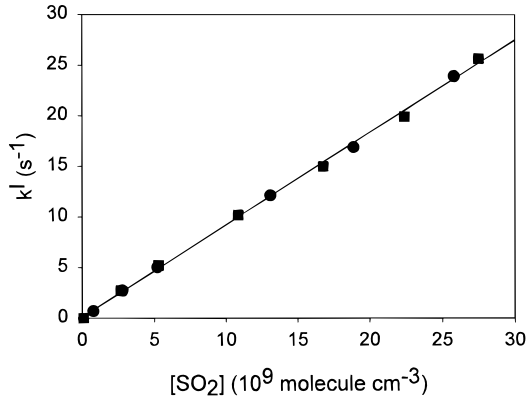

Figure 5. First-order rate coefficient for the loss of SF_6^- as a function of the concentration of SO_2 in the ion trap for two different trapping voltages (squares = $290V_{p-p}$; circles = $570V_{p-p}$) in 2.2 mTorr He.

through a 50 cm long by 2.5 cm i.d. Pyrex absorption cell fitted with quartz windows and through an 1/8 in. o.d. Teflon tube into the ion trap chamber. The HNO_3 concentration was measured by absorption of the 185 nm Hg line ($\sigma = 1.63 \times 10^{-17}$ cm^2 $molecule^{-1}$)[16] using techniques very similar to those described by Huey et al.[17] The absorption cell pressure was regulated by constricting the flow through the Teflon tubing with a pinch clamp.

The concentrations of SO_2 and HCl in the ion trap were determined by measuring the flow rates of the gases into the ion trap chamber. The gas mixtures of SO_2 and HCl with He were prepared in Pyrex bulbs and calibrated by absorption measurements (SO_2: Zn 214 nm, $\sigma = 3.87 \times 10^{-18}$ cm^2 $molecule^{-1}$)[18] (HCl: Hg 185 nm, $\sigma = 3.2 \times 10^{-19}$ cm^2 $molecule^{-1}$).[19]

Relative rate coefficients were also measured for reactions of the product ions from the SF_6^- reactions with SO_2, HNO_3, and HCl. For example, the rate coefficients for the reactions of $F_2SO_2^-$ and SF_5^- with SO_2 were measured relative to the $SF_6^- + SO_2$ rate coefficient by simultaneously generating SF_6^-, $F_2SO_2^-$, and SF_5^- in the ion−molecule reactor and then independently isolating the individual ions in the trap and comparing their first-order losses for the same concentration of SO_2. This was repeated for several SO_2 concentrations. Kinetic results for the reactions of product ions from SF_6^- reactions with SO_2, HNO_3, and HCl are summarized in Table 1. All of the rate coefficients reported in Table 1 were measured with rf trapping voltages of $290V_{p-p}$ ($q_z = 13.9$/m(amu)) during the

TABLE 1: Ion−Molecule Rate Coefficients and Product Yields

	yield		total rate coefficient[a] (10^{-9} cm^3 molecule^{-1} s^{-1})	
reaction	this work	literature	this work	literature
$SF_6^- + SO_2 \rightarrow F_2SO_2^- + SF_4$	0.57	0.54[b]	0.9	1.0[b,c,d]
$\rightarrow SF_5^- + FSO_2$	0.27	0.26		
$\rightarrow FSO_2^- + SF_5$	0.16	0.20		
$F_2SO_2^- + SO_2 \rightarrow FSO_2^- + FSO_2$			(0.3)	
$SF_5^- + SO_2 \rightarrow FSO_2^- + SF_4$			(0.6)	
$SF_5Cl^- + SO_2 \rightarrow$			(<0.01)	
$NO_3^-\cdot HF + SO_2 \rightarrow$			(<0.01)	
$NO_3^-\cdot HNO_3 + SO_2 \rightarrow$			(<0.01)	
$SF_6^- + HNO_3 \rightarrow NO_3^-\cdot HF + SF_5$	0.91	0.92[b]	1.9	2.0[b]
$\rightarrow SF_5^- + HF + NO_3$	0.06	0.05		
$\rightarrow SF_5NO_3^- + HF$	0.02	0.02		
$\rightarrow NO_3^- + HF + SF_5$	0.01	0.01		
$NO_3^-\cdot HF + HNO_3 \rightarrow NO_3^-\cdot HNO_3 + HF$			(1.9)	
$SF_5^- + HNO_3 \rightarrow NO_3^-\cdot HF + SF_4$			(2.1)	
$FSO_2^- + HNO_3 \rightarrow NO_3^-\cdot HF + SO_2$			(1.7)	
$F_2SO_2^- + HNO_3 \rightarrow NO_3^-\cdot HF + FSO_2$	0.75		(1.9)	
$\rightarrow FSO_3^- + HF + NO_2$	0.25			
$SF_5Cl^- + HNO_3 \rightarrow NO_3^-\cdot HF + SF_4Cl$	0.60		(1.5)	
$\rightarrow ClNO_3^-\cdot HF + SF_4$	0.40			
$SF_6^- + HCl \rightarrow SF_5Cl^- + HF$	0.66	0.44[b]	1.2	1.5[b], 0.4[d]
$\rightarrow SF_5^- + HF + Cl$	0.26	0.33		
$\rightarrow Cl^-\cdot HF + SF_5$	0.08	0.23		
$FSO_2^- + HCl \rightarrow Cl^-\cdot HF + SO_2$	0.60	0.5[e]	(1.2)	0.3[e]
$\rightarrow ClSO_2^- + HF$	0.40	0.5		
$F_2SO_2^- + HCl \rightarrow FClSO_2^- + HF$	0.94		(1.3)	
$\rightarrow Cl^-\cdot HF + FSO_2$	0.06			
$SF_5^- + HCl \rightarrow SF_4Cl^- + HF$	0.75		(1.2)	
$\rightarrow Cl^-\cdot HF + SF_4$	0.25			
$ClSO_2^- + HCl \rightarrow Cl^-\cdot HCl + SO_2$			[0.9]	
$Cl^-\cdot HF + HCl \rightarrow Cl^-\cdot HCl + HF$			[0.7]	
$NO_3^-\cdot HNO_3 + HCl \rightarrow$			(<0.01)	
$NO_3^-\cdot HF + HCl \rightarrow NO_3^-\cdot HCl + HF$			(0.8)	

[a] Rate coefficients in parentheses were measured relative to SF_6^- and rate coefficients in square brackets were measured relative to FSO_2^-. [b] Ref 17. [c] Ref 28. [d] Ref 29. [e] Ref 22.

reaction period. The estimated uncertainty in the rate coefficients is ±20%.

Product ion yields are reported for reactions with more than one product channel. The reported yields are the ratios of the observed product ion signals at short reaction time. In most cases the sum of the product ion signals was within 30% of the reactant ion loss, suggesting that mass discrimination is probably not severe. The estimated uncertainty in the product yields is ±30% of the yield.

$NO_3^-(HNO_3)_2$ Decomposition. The decomposition of the $NO_3^-(HNO_3)_2$ cluster ion was studied in the ion trap. $NO_3^-(HNO_3)_2$ was generated in the ion−molecule reactor by the following sequence of reactions:

$$SF_6^- + HNO_3 \rightarrow NO_3^-\cdot HF + SF_5 \quad (2)$$

$$NO_3^-\cdot HF + HNO_3 \rightarrow NO_3^-\cdot HNO_3 + HF \quad (3)$$

$$NO_3^-\cdot HNO_3 + HNO_3 + M \rightleftarrows NO_3^-(HNO_3)_2 + M \quad (4)$$

An example of the decay of $NO_3^-(HNO_3)_2$ and the production of $NO_3^-\cdot HNO_3$ as a function of delay following selective trapping of $NO_3^-(HNO_3)_2$ is shown in Figure 6. The observed loss of $NO_3^-(HNO_3)_2$ is a combination of reactive and nonreactive processes. The extent of nonreactive loss of stable ions (e.g., $NO_3^-\cdot HNO_3$ and SF_6^-) from the trap is small (<0.01 s^{-1}). Therefore, it is assumed that the nonreactive loss of $NO_3^-(HNO_3)_2$ is also less than 0.01 s^{-1}. The pseudo-first-order rate coefficient for loss of $NO_3^-(HNO_3)_2$ increased linearly with pressure over the range 0.2−2 mTorr for a trapping voltage of $290V_{p-p}$ (q_z = 0.074). The pseudo-first-order rate coefficient for loss of $NO_3^-(HNO_3)_2$ was also a weak linear function of the rf trapping voltage, increasing from 0.8 to 1.2 s^{-1} over the range 290−$2220V_{p-p}$ (q_z ranging from 0.074 to 0.566) in 1.8 mTorr He. The first-order rate coefficient for the loss of $NO_3^-(HNO_3)_2$ was also a function of the concentration of added N_2. The variation of the pseudo-first-order rate coefficient as a function of the fraction of N_2 for two different trapping voltages is shown in Figure 7.

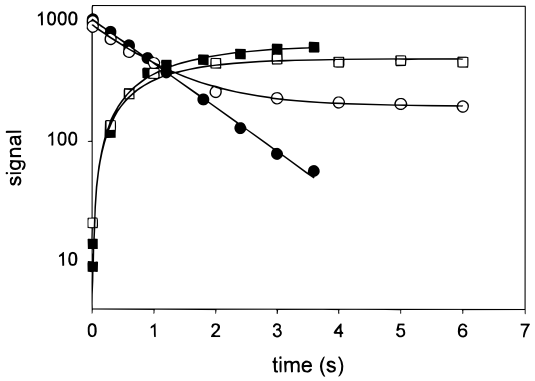

Figure 6. Decay of $NO_3^-\cdot(HNO_3)_2$ (circles) and appearance of $NO_3^-\cdot HNO_3$ (squares) as a function of time for $[HNO_3] = 0$ (filled symbols) and $[HNO_3] = 9 \times 10^{10}$ molecule cm^{-3} (open symbols) in 1.7 mTorr He. The lines are fits to the data.

The decay of $NO_3^-(HNO_3)_2$ was also measured in the presence of HNO_3 to determine an effective equilibrium constant for reaction 4 in the ion trap. An example of the decay of $NO_3^-(HNO_3)_2$ and the appearance of $NO_3^-\cdot HNO_3$ with added

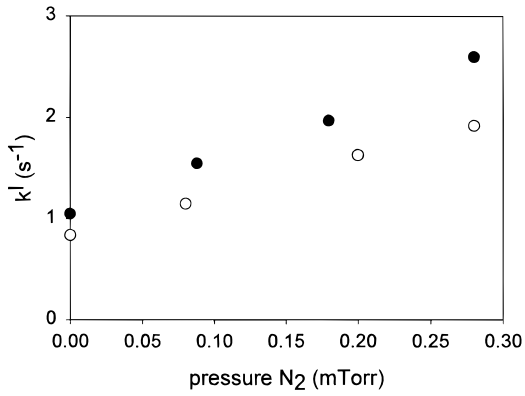

Figure 7. Variation of the first-order rate coefficient for $NO_3^-(HNO_3)_2$ decomposition as a function of the partial pressure of N_2 and trapping voltage (open circles = $290V_{p-p}$; filled circles = $570V_{p-p}$). Total trap pressure was held constant at 1.7 mTorr (He + N_2).

HNO_3 is shown in Figure 6. The solid lines are fits to the data using the analytical expression for the temporal dependence of two species approaching equilibrium. Fits to these type of data yield an effective equilibrium constant in the trap of 2.4×10^{-12} cm^3 $molecule^{-1}$, which was independent of pressure from 1.0 to 2.6 mTorr He for an rf trapping potential of $290V_{p-p}$ (q_z = 0.074). The equilibrium constant decreased to 1.2×10^{-12} cm^3 $molecule^{-1}$ when the trapping voltage was increased to $1120V_{p-p}$ (q_z = 0.286) with He buffer gas.

The equilibrium constant was also measured as a function of added N_2. The equilibrium constant decreased to 1.3×10^{-12} cm^3 $molecule^{-1}$ when 10% of the buffer gas in the ion trap chamber was N_2 with a trap pressure of 1.8 mTorr and a trapping voltage of $290V_{p-p}$ (q_z = 0.074).

$NO_3^-\cdot HNO_3 + HNO_3 + M \rightarrow NO_3^-(HNO_3)_2 + M$. Rate coefficients for the association reaction between $NO_3^-\cdot HNO_3$ and HNO_3 were measured in the ion trap. $NO_3^-\cdot HNO_3$ was generated in the ion−molecule reactor by reactions 2 and 3 and selectively trapped. The decay of $NO_3^-\cdot HNO_3$ ion was monitored as a function of time in the presence of HNO_3 with a noise field applied to the end caps to continuously eject the $NO_3^-(HNO_3)_2$ product. In this way the association reaction could be studied independently from the decomposition of $NO_3^-(HNO_3)_2$. The kinetic results are summarized in Table 2. The second-order association rate coefficient increased linearly with ion trap pressure from 0.7 to 2.0 mTorr He as expected for a three-body association reaction. The association rate coefficient decreased by a factor of 2 when the trapping potential was increased from 290 to $1120V_{p-p}$ (q_z increased from 0.111 to 0.430).

$NO_3^- + HNO_3 + M \rightarrow NO_3^-\cdot HNO_3 + M$. The rate coefficient for the association reaction between NO_3^- and HNO_3 was measured in the ion trap. NO_3^- was generated in the flowing afterglow reactor by electron attachment to HNO_3.[20]

$$HNO_3 + e^- \rightarrow NO_2^- + OH \quad (5)$$

$$NO_2^- + HNO_3 \rightarrow NO_3^- + HONO \quad (6)$$

and was selectively trapped with a FNF applied during the trapping period. The pseudo-first-order decay of NO_3^- was measured for a range of HNO_3 concentrations. The decays were exponential, suggesting that the $NO_3^-\cdot HNO_3$ decomposition is slow. This is consistent with the observation that $NO_3^-\cdot HNO_3$ has a very long lifetime in the trap (>100 s). The kinetic results are summarized in Table 2.

$NO_3^-\cdot HNO_3 + HNO_3 + M \rightleftarrows NO_3^-(HNO_3)_2 + M$ Equilibrium Constant. The equilibrium constant for the reaction $NO_3^-\cdot HNO_3 + HNO_3 + M \rightleftarrows NO_3^-(HNO_3)_2 + M$ was measured in the ion−molecule reactor under thermal conditions for comparison with the ion trap results. $NO_3^-\cdot HNO_3$ was generated in the upstream end of the ion−molecule reactor by reacting SF_6^- with HNO_3 (reactions 2 and 3). HNO_3 was added to the reactor 20 cm downstream of the electron source and 50 cm upstream of the ion-sampling orifice. At equilibrium the ion concentrations are given by

$$K_c = \frac{[NO_3^-(HNO_3)_2]}{[NO_3^-\cdot HNO_3][HNO_3]} = 1.362 \times 10^{-22} T \exp\left(\frac{-\Delta G^\circ}{RT}\right) \quad (7)$$

where ΔG° is the standard Gibbs free energy change for the reaction, R is the gas constant, and the units of K_c are cm^3 $molecule^{-1}$. The equilibrium constant was measured by adding known concentrations of HNO_3 to the ion−molecule reactor and measuring the ratio of the $NO_3^-(HNO_3)_2$ and $NO_3^-\cdot HNO_3$ ion signals. The ratio of the ion signals is related to the ratio of the ion concentrations by the relative detection sensitivity. The relative sensitivity was measured by monitoring the change in the $NO_3^-\cdot HNO_3$ and $NO_3^-(HNO_3)_2$ signals as $[HNO_3]$ was varied. The mass spectrometer was about 1.2 times more sensitive to $NO_3^-(HNO_3)_2$ than $NO_3^-\cdot HNO_3$ for the trapping conditions used in the equilibrium measurements (1.4 mTorr He, trapping potential of $290V_{p-p}$, trap time = 20 ms). For the ion−molecule reactor conditions (100 STP cm^3 s^{-1}, 20 Torr He at 303 K and 10 Torr at 322 K) the measured equilibrium constants were independent (less than 30% variation) of $[HNO_3]$ ($(0.9-4) \times 10^{11}$ molecule cm^{-3} at 303 K, $(0.5-4) \times 10^{12}$ molecule cm^{-3} at 322 K). The measured equilibrium constants are 8.6×10^{-12} cm^3 $molecule^{-1}$ at 303 K and 1.3×10^{-12} cm^3 $molecule^{-1}$ at 322 K, with an estimated uncertainty of about ±30%.

Discussion

SF_6^- and Product Ion Kinetic Measurements in the Ion Trap. The rate coefficients for the reactions of SF_6^- with SO_2, HNO_3, and HCl measured in the ion trap are in very good agreement with the recent room-temperature flowing afterglow results of Huey et al.[17] These reactions all proceed at the collision rate and are not expected to be influenced strongly by translational energy excitation.[21] $F_2SO_2^-$ and SF_5^- react slightly slower than the collision rate with SO_2 and mainly by fluoride transfer. No reactions between SO_2 and SF_5Cl^-, $NO_3^-\cdot HF$, and $NO_3^-\cdot HNO_3$ were observed. SF_5^-, FSO_2^-, $F_2SO_2^-$, and SF_5Cl^- react with HNO_3 at or near the collision rate, mainly by fluoride transfer. HCl reacts with FSO_2^-, SF_5^-, $ClSO_2^-$, and $Cl^-\cdot HF$ at near the collision rate, and the production of HF is favored when possible. The FSO_2^- + HCl rate coefficient measured in the present work is significantly larger than the value reported by Sullivan and Beauchamp[22] measured in an ion cyclotron mass spectrometer.

The measured product yields for the reactions of SF_6^- with SO_2 and HNO_3 are in very good agreement with the Huey et al.[17] work. However, a significantly smaller yield of $Cl^-\cdot HF$ is observed in the present study for the SF_6^- + HCl reaction than reported by Huey et al. The product yields for FSO_2^- + HCl are in good agreement with the Sullivan and Beauchamp[22] work.

$NO_3^-(HNO_3)_x$ Reactions. The third-order rate coefficient measured in the ion trap for the reaction $NO_3^- + HNO_3 + He$ (3.1×10^{-26} cm^6 $molecule^{-2}$ s^{-1}) is consistent with the lower

TABLE 2: $NO_3^-(HNO_3)_x$ Rate Coefficients[a]

reaction	trap pressure (mTorr He)	pressure-independent rate coefficient
$NO_3^- + HNO_3 + He \rightarrow NO_3^-\cdot HNO_3 + He$	1.75	3.1×10^{-26} cm^6 molec.$^{-2}$ s^{-1}
$NO_3^-\cdot HNO_3 + He \rightarrow NO_3^- + HNO_3 + He$	1.80	$< 2 \times 10^{-16}$ cm^3 molec.$^{-1}$ s^{-1}
$NO_3^-\cdot HNO_3 + HNO_3 + He \rightarrow NO_3^-(HNO_3)_2 + He$	0.7−2.0	3.9×10^{-26} cm^6 molec.$^{-2}$ s^{-1}
$NO_3^-(HNO_3)_2 + He \rightarrow NO_3^-\cdot HNO_3 + HNO_3 + He$	0.2−2.0	1.6×10^{-14} cm^3 molec.$^{-1}$ s^{-1}

[a] 298 K, $290V_{p-p}$ trapping potential.

limit of 1×10^{-26} cm^6 molecule^{-2} s^{-1} reported by Fehsenfeld et al.[20] for an N_2 flowing afterglow experiment.

There is very good agreement between the equilibrium constant for the reaction $NO_3^-\cdot HNO_3 + HNO_3 \rightleftarrows NO_3^-\cdot(HNO_3)_2$ measured in the ion trap by monitoring the equilibration of $NO_3^-\cdot(HNO_3)_2$ in the presence of HNO_3 and the equilibrium constant determined from individual measurements of the forward and reverse rate coefficients. This result strongly supports the value measured for the association rate coefficient by using a filtered noise field to continuously eject the unstable $NO_3^-\cdot(HNO_3)_2$ product.

The equilibrium constants measured for the reaction $NO_3^-\cdot HNO_3 + HNO_3 \rightleftarrows NO_3^-\cdot(HNO_3)_2$ for thermal conditions in the ion−molecule reactor are in good agreement with the flowing afterglow results of Davidson et al.,[23] who reported $\Delta H^\circ = -18.3 \pm 1.0$ kcal mol^{-1} and $\Delta S^\circ = -22.1 \pm 2$ cal mol^{-1} K^{-1}, giving $K_c = 9.7 \times 10^{-12}$ cm^3 molecule^{-1} at 303 K and 1.7×10^{-12} at 322 K. An effective temperature for the trapped $NO_3^-\cdot(HNO_3)_2$ ion may be derived from the measurements of the equilibrium constant and the known thermodynamics for the reaction $NO_3^-\cdot HNO_3 + HNO_3 \rightleftarrows NO_3^-\cdot(HNO_3)_2$. The equilibrium measurements in the trap yield $K_c = 2.4 \times 10^{-12}$ cm^3 molecule^{-1}, which translates to an effective temperature for the trapped ions (1−2 mTorr He, 298 K, trapping voltage = 290, $q_z = 0.074$) of 318 K using the Davidson et al. thermodynamics. The effective ion temperature increased to 325 K with 10% added N_2 (He + N_2 pressure = 1.8 mTorr). The increase in the ion internal energy in the presence of a small amount of a heavier buffer gas is consistent with drift tube studies that show that the ion internal energy increases in heavier buffer gases.[24] The effective ion temperature also increased to about 325 K when the trapping potential was increased to $1120V_{p-p}$ ($q_z = 0.286$). The uncertainty in the measured ion temperature is estimated to be about ±30 K on the basis of estimated uncertainties of ±1 kcal mol^{-1} in ΔG° and 50% in the measured equilibrium constant.

It should be recognized that the equilibrium relationship (eq 7) used to derive the effective ion temperature is based on a Boltzmann distribution of energy in the ion. It is very unlikely that the trapped ions have a Boltzmann distribution of energy because of the translational excitation by the trapping potential. However, the low effective temperatures measured in the present work do suggest that the internal energy of the trapped ion is close to thermal.

The effective ion temperature measured in the present work is significantly lower than the 530−720 K temperature derived by Nourse and Kenttamaa[7] from observations of the decomposition of polyatomic ions in a He buffered ion trap. However, the temperature dependence for the decomposition rate coefficient used in that study is probably inappropriate. Nourse and Kenttamaa[7] assumed that the temperature dependence of the pressure-independent decomposition rate coefficient is given by

$$k(T) = k_{capture} \exp\left(\frac{-E_a}{RT}\right) \tag{8}$$

which only holds approximately for endothermic bimolecular reactions and should not be applied to association/decomposition reactions. Equation 8 is derived by considering a generalized bimolecular reaction

$$A + B \rightleftarrows C + D \qquad (k_{fb}, k_{rb}) \tag{9}$$

which is exothermic as written; that is, k_{rb} is the rate coefficient for the endothermic reaction of $C + D \rightarrow A + B$. Then, noting that the equilibrium constant equals the ratio of the forward and reverse rate coefficients yields

$$k_{rb} = k_{fb} \exp\left(\frac{\Delta G^\circ}{RT}\right) = k_{fb} \exp\left(\frac{-\Delta S^\circ}{R}\right) \exp\left(\frac{\Delta H^\circ}{RT}\right) \tag{10}$$

If the forward exothermic reaction proceeds at the capture rate, and the entropy change is negligible, eq 10 reduces to eq 8.

The temperature dependence of a decomposition reaction is derived from the equilibrium constant for the general reaction

$$C + M \rightleftarrows A + B + M \qquad (k_d, k_a) \tag{11}$$

where the decomposition (k_d) and association (k_a) rate coefficients are either both pressure dependent or pressure independent. Employing eq 7, the decomposition rate coefficient is written as

$$k_d = \frac{k_a \exp\left(\frac{\Delta S^\circ}{R}\right) \exp\left(\frac{-\Delta H^\circ}{RT}\right)}{1.362 \times 10^{-22} T} \tag{12}$$

where the rate coefficients have molecular units (i.e., k_a/k_d [=] cm^3 molecule^{-1}). This equation can be used to reevaluate the Nourse and Kenttamaa data. Upper limits on the effective internal temperature of the ions may be estimated by using limits of $k_a > 1 \times 10^{-31}$ cm^6 molecule^{-2} s^{-1} and $\Delta S^\circ > 20$ cal mol^{-1} K^{-1}, with $\Delta H^\circ = 11.5$ kcal mol^{-1}.[7] Nourse and Kenttamaa[7] report half-lives for protonated cyclohexene oxide and tetraethylsilane of 600 and 300 ms in the ion trap with 5 mTorr He, giving pressure-independent decomposition rate coefficients of 7×10^{-15} and 1.4×10^{-14} cm^3 molecule^{-1} s^{-1}. Using these rate coefficients and the limits suggested above for k_a and ΔS° yields effective temperatures of <368 and <386 K for protonated cyclohexene oxide and tetraethylsilane, respectively. These temperature limits are consistent with the temperature measured in this work, but are significantly lower than the temperatures reported by Nourse and Kenttamaa.[7]

McLuckey et al.[11] deduced effective internal ion temperatures for protonated water and methanol clusters from analysis of the ion desolvation kinetics in the ion trap. They also used eq 8 to extract the ion temperatures. To extract temperatures by using eq 12, rate coefficients for the clustering reactions (k_a) are needed. Several of the clustering rate coefficients have been measured for thermal conditions. In particular, using pressure-independent association rate coefficients of 1×10^{-29} [25] and 1.5×10^{-27} cm^6 molecule^{-2} s^{-1} [26] for the reactions $H_3O^+(H_2O)_3 + H_2O + H_2$ and $H_3O^+(H_2O)_2 + H_2O + He$, respectively, and the known thermodynamics,[27] temperatures of 410 and 363 K are determined for $H_3O^+(H_2O)_3$ (1.2 mTorr) and $H_3O^+(H_2O)_2$

(0.74 mTorr) ions. These temperatures are slightly higher than the $NO_3^-(HNO_3)_2$ temperature measured in the present work.

McLuckey et al.[11] observed that the bimolecular decomposition rate constants for the protonated water and methanol clusters decreased as the He bath gas pressure increased over the range 0.02−1.2 mTorr. They attributed the decrease to an increase in the internal ion temperature at lower bath gas pressures. In contrast, in the present work, the bimolecular rate coefficient for the decomposition of $NO_3^-(HNO_3)_2$ is independent of pressure over the range 0.2−2.0 mTorr.

A lower limit of 1.6×10^{-10} cm^3 molecule^{-1} for the equilibrium constant for $NO_3^- + HNO_3 \leftrightarrow NO_3^-\cdot HNO_3$ in the ion trap can be derived from the forward and reverse rate coefficients listed in Table 2. Using this equilibrium constant and an effective ion temperature of 320 K gives $\Delta G°_{320\ K} < -14$ kcal mol^{-1} for this reaction. This is consistent with the flowing afterglow limit reported by Davidson et al.[23] ($\Delta G°_{367\ K} < -14.5$ kcal mol^{-1}).

Acknowledgment. E.R.L. is grateful to Greg Huey, Dave Hanson, Carl Howard, Roger Van Zee, Tim Onster, Phillip Hemberger, and Greg Eiden for useful discussions. Carl Howard suggested the ion trap conductance phenomenon, and Greg Huey provided useful comments on the manuscript. The assistance from R. M. Jordan during the construction of the apparatus is also greatly appreciated.

References and Notes

(1) Paul, W.; Steinwedel, H. U.S. Patent 2939952, 1960.

(2) See, for example: March, R. E.; Hughes, R. J. *Quadrupole Storage Mass Spectrometry*; Wiley: New York, 1989. *Practical Aspects of Ion Trap Mass Spectrometry*; March, R. E., Todd, J. F. J., Eds.; CRC: Boca Raton, 1995; Vol. I−III.

(3) March, R. E.; Hughes, R. J. *Quadrupole Storage Mass Spectrometry*; Wiley: New York, 1989; Chapter 3, p 150.

(4) Vedel, F. *Int. J. Mass Spectrom. Ion Processes* **1991**, *106*, 33.

(5) Schaaf, H.; Schmeling, U.; Werth, G. *Appl. Phys.* **1981**, *25*, 249.

(6) Cutler, L. S.; Flory, C. A.; Giffard, R. P.; McGuire, M. D. *Appl. Phys. B* **1986**, *39*, 251.

(7) Nourse, B. D.; Kenttamaa, H. I. *J. Phys. Chem.* **1990**, *94*, 5809.

(8) Dotan, I.; Fehsenfeld, F. C.; Albritton, D. L. *J. Chem. Phys.* **1978**, *68*, 5665. Albritton, D. L. In *Kinetics of Ion−Molecule Reactions*; Ausloos, P., Ed.; Plenum Press: New York, 1979.

(9) Basic, C.; Eyler, J. R.; Yost, R. A. *J. Am. Soc. Mass Spectrom.* **1992**, *3*, 716.

(10) Brodelt-Lustig, J. S.; Cooks, R. G. *Talanta* **1989**, *36*, 255.

(11) McLuckey, S. A.; Glish, G. L.; Asano, K. G.; Bartmess, J. E. *Int. J. Mass Spectrosc. Ion. Processes* **1991**, *109*, 171.

(12) Lunney, M. D. N.; Buchinger, F.; Moore, R. B. *J. Mod. Opt.* **1992**, *39*, 349.

(13) Poulter, K. F.; Rodgers, M.-J.; Nash, P. J.; Thompson, T. J.; Perkins, M. P. *Vacuum* **1983**, *33*, 311.

(14) See, for example: Chen, L.; Wang, T. C. L.; Ricca, T. L.; Marshall, A. G. *Anal. Chem.* **1987**, *59*, 449. Soni, M.; Cooks, R. G. *Anal. Chem.* **1994**, *66*, 2488. Goeringer, D. E.; Asano, K. G.; McLuckey, S. A.; Hoekman, D.; Stiller, S. W. *Anal. Chem.* **1994**, *66*, 313.

(15) Brown, G. P.; DiNardo, A.; Cheng, G. K.; Sherwood, T. K. *J. Appl. Phys.* **1946**, *17*, 802.

(16) Biaume, F. *J. Photochem.* **1973**, *2*, 139.

(17) Huey, L. G.; Hanson, D. R.; Howard, C. J. *J. Phys. Chem.* **1995**, *99*, 5001.

(18) Wine, P. H.; Thompson, R. J.; Ravishankara, A. R.; Semmes, D. H.; Gump, C. A.; Torabi, A.; Nicovich, J. M. *J. Phys. Chem.* **1984**, *88*, 2095.

(19) Inn, E. C. Y. *J. Atmos. Sci.* **1975**, *32*, 2375.

(20) Fehsenfeld, F. C.; Howard, C. J.; Schmeltekopf, A. L. *J. Chem. Phys.* **1975**, *63*, 2835.

(21) Dotan, I.; Lindinger, W.; Rowe, B.; Fahey, D. W.; Fehsenfeld, F. C.; Albritton, D. L. *Chem. Phys. Lett.* **1980**, *72*, 67.

(22) Sullivan, S. A.; Beauchamp, J. L. *Int. J. Mass Spectrom. Ion Phys.* **1978**, *28*, 69.

(23) Davidson, J. A.; Fehsenfeld, F. C.; Howard, C. J. *Int. J. Chem. Kinet.* **1977**, *9*, 17.

(24) Albritton, D. L. In *Kinetics of Ion−Molecule Reactions;* Ausloos, P., Ed.; Plenum Press: New York, 1979. Lindinger, W.; McFarland, M.; Fehsenfeld, F. C.; Albritton, D. L.; Schmeltekopf, A. L.; Ferguson, E. E. *J. Chem. Phys.* **1975**, *63*, 2175.

(25) Burt, J. A.; Dunn, J. L.; McEwan, M. J.; Sutton, M. M.; Roche, A. E.; Schiff, H. I. *J. Chem. Phys.* **1970**, *52*, 6062.

(26) Bierbaum, V. M.; Golde, M. F.; Kaufman, F. *J. Chem. Phys.* **1976**, *65*, 2715.

(27) Grimsrud, E. P.; Kebarle, P. *J. Am. Chem. Soc.* **1973**, *95*, 7939.

(28) Ferguson, E. E. *Int. J. Mass Spectrom. Ion Phys.* **1976**, *19*, 53

(29) Streit, G. E. *J. Chem. Phys.* **1982**, *77*, 826.